Brief Communication

Cell Chemical Biology

Discovery of an AKT Degrader with Prolonged Inhibition of Downstream Signaling

Graphical Abstract

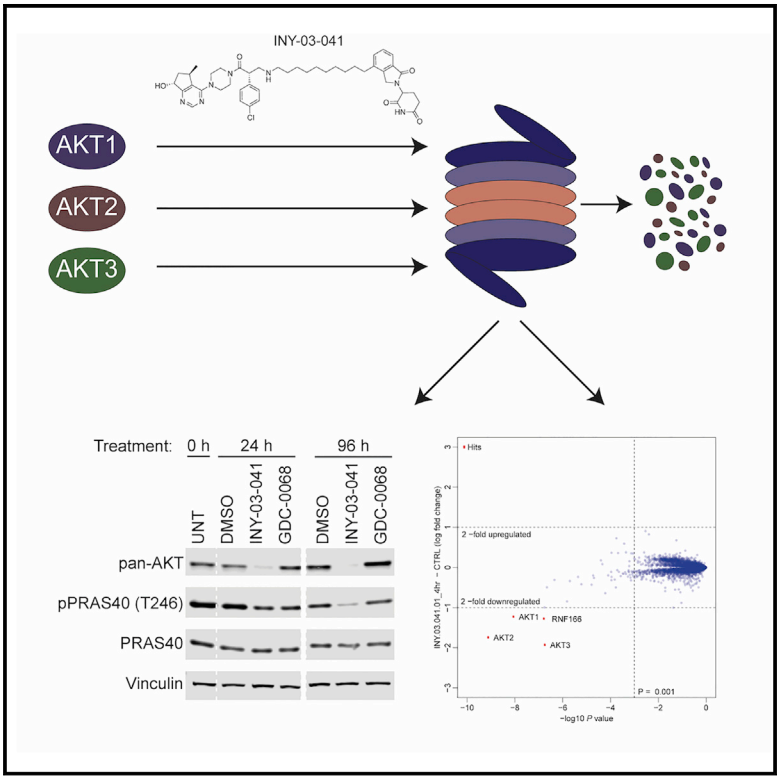

Highlights

- An AKT-selective heterobifunctional degrader was developed
- AKT degradation induced stronger anti-proliferative effects than AKT inhibition
- AKT loss and inhibition of downstream signaling was sustained, even after washout

Authors

Inchul You, Emily C. Erickson, Katherine A. Donovan, Nicholas A. Eleuteri, Eric S. Fischer, Nathanael S. Gray, Alex Toker

Correspondence

nathanael_gray@dfci.harvard.edu (N.S.G.), atoker@bidmc.harvard.edu (A.T.)

In Brief

You and Erickson et al. report the development and characterization of INY-03-041, a highly selective AKT degrader. The authors demonstrate that INY-03-041 not only exhibits more potent anti-proliferative effects than the catalytic inhibitor GDC-0068, but also induces sustained AKT destabilization and inhibition of downstream signaling, even after compound washout.

You et al., 2020, Cell Chemical Biology *27*, 1–8
January 16, 2020
https://doi.org/10.1016/j.chembiol.2019.11.014

CellPress

Please cite this article in press as: You et al., Discovery of an AKT Degrader with Prolonged Inhibition of Downstream Signaling, Cell Chemical Biology (2019), https://doi.org/10.1016/j.chembiol.2019.11.014

Cell Chemical Biology

Brief Communication

CellPress

Discovery of an AKT Degrader with Prolonged Inhibition of Downstream Signaling

Inchul You,[1,2,4] Emily C. Erickson,[3,4] Katherine A. Donovan,[1,2] Nicholas A. Eleuteri,[1] Eric S. Fischer,[1,2] Nathanael S. Gray,[1,2,*] and Alex Toker[3,5,*]

[1]Department of Cancer Biology, Dana-Farber Cancer Institute, Boston, MA 02215, USA

[2]Department of Biological Chemistry and Molecular Pharmacology, Harvard Medical School, Boston, MA 02215, USA

[3]Department of Pathology, Medicine and Cancer Center, Beth Israel Deaconess Medical Center, Harvard Medical School, Boston, MA 02215, USA

[4]These authors contributed equally

[5]Lead Contact

*Correspondence: nathanael_gray@dfci.harvard.edu (N.S.G.), atoker@bidmc.harvard.edu (A.T.)

https://doi.org/10.1016/j.chembiol.2019.11.014

SUMMARY

The PI3K/AKT signaling cascade is one of the most commonly dysregulated pathways in cancer, with over half of tumors exhibiting aberrant AKT activation. Although potent small-molecule AKT inhibitors have entered clinical trials, robust and durable therapeutic responses have not been observed. As an alternative strategy to target AKT, we report the development of INY-03-041, a pan-AKT degrader consisting of the ATP-competitive AKT inhibitor GDC-0068 conjugated to lenalidomide, a recruiter of the E3 ubiquitin ligase substrate adaptor Cereblon (CRBN). INY-03-041 induced potent degradation of all three AKT isoforms and displayed enhanced anti-proliferative effects relative to GDC-0068. Notably, INY-03-041 promoted sustained AKT degradation and inhibition of downstream signaling effects for up to 96 h, even after compound washout. Our findings suggest that AKT degradation may confer prolonged pharmacological effects compared with inhibition, and highlight the potential advantages of AKT-targeted degradation.

INTRODUCTION

The serine/threonine kinase AKT is a central component of the phosphoinositide 3-kinase (PI3K) signaling cascade and is a key regulator of critical cellular processes, including proliferation, survival, and metabolism (Manning and Toker, 2017). The AKT protein kinase family comprises three highly homologous isoforms, AKT1, AKT2, and AKT3, that possess both redundant functions and isoform-specific activities (Toker, 2012). Hyperactivation of AKT, due to gain-of-function mutations or amplification of oncogenes (receptor tyrosine kinases and PI3K) or inactivation of tumor suppressor genes (PTEN, INPP4B, and PHLPP), is one of the most common molecular perturbations in cancer and promotes malignant phenotypes associated with tumor initiation and progression (Cantley and Neel, 1999; Fruman et al., 2017; Shayesteh et al., 1999). Thus, AKT is an attractive therapeutic target and significant efforts have been made to develop AKT-targeted therapies (Brown and Banerji, 2017).

Current strategies to target AKT have focused on ATP-competitive, allosteric, and covalent inhibitors. Several ATP-competitive inhibitors, such as ipatasertib (GDC-0068) and capivasertib (AZD5363), are currently under clinical investigation in phase II and III studies (Oliveira et al., 2019; Turner et al., 2019). However, these inhibitors suffer from a lack of selectivity among the AGC kinase family, and this may limit their clinical efficacy or tolerability (Huck and Mochalkin, 2017). By contrast, allosteric inhibitors which target the pleckstrin homology domain, such as MK-2206 and miransertib (ARQ-092), exhibit a high degree of specificity toward AKT, but either lack significant efficacy in the clinic or require further clinical evaluation (Do et al., 2015; Keppler-Noreuil et al., 2019). Covalent allosteric inhibitors which target AKT at Cys296 and Cys310 have been reported, but have not advanced to clinical trials (Uhlenbrock et al., 2019).

An alternative pharmacological approach to inhibiting AKT activity is to directly reduce cellular AKT protein levels via targeted protein degradation. Heterobifunctional degraders, also known as proteolysis targeting chimeras, consist of a moiety that binds to an E3 ubiquitin ligase chemically linked to a second moiety that engages a target protein, thereby recruiting the E3 ligase into close proximity to the target protein to induce its ubiquitination and subsequent proteasomal degradation (Winter et al., 2015). Several advantages of degraders over inhibitors have been reported, which include enhancing the selectivity of multi-targeted inhibitors (CDK9) (Olson et al., 2018), abrogating non-kinase-dependent functions (FAK) (Cromm et al., 2018), and overcoming resistance mutations (BTK) (Dobrovolsky et al., 2018). Because the pharmacological effects of degraders depend on the re-synthesis rate of the target protein rather than sustained target occupancy, small-molecule degraders may also have significantly prolonged effects in comparison with reversible inhibitors. However, while the potential for degraders to achieve an extended pharmacological duration of action has been noted, there have been no reported degraders to date that highlight such a feature (Churcher, 2018). Given the long half-life of AKT (Basso et al., 2002) and its importance in cancer

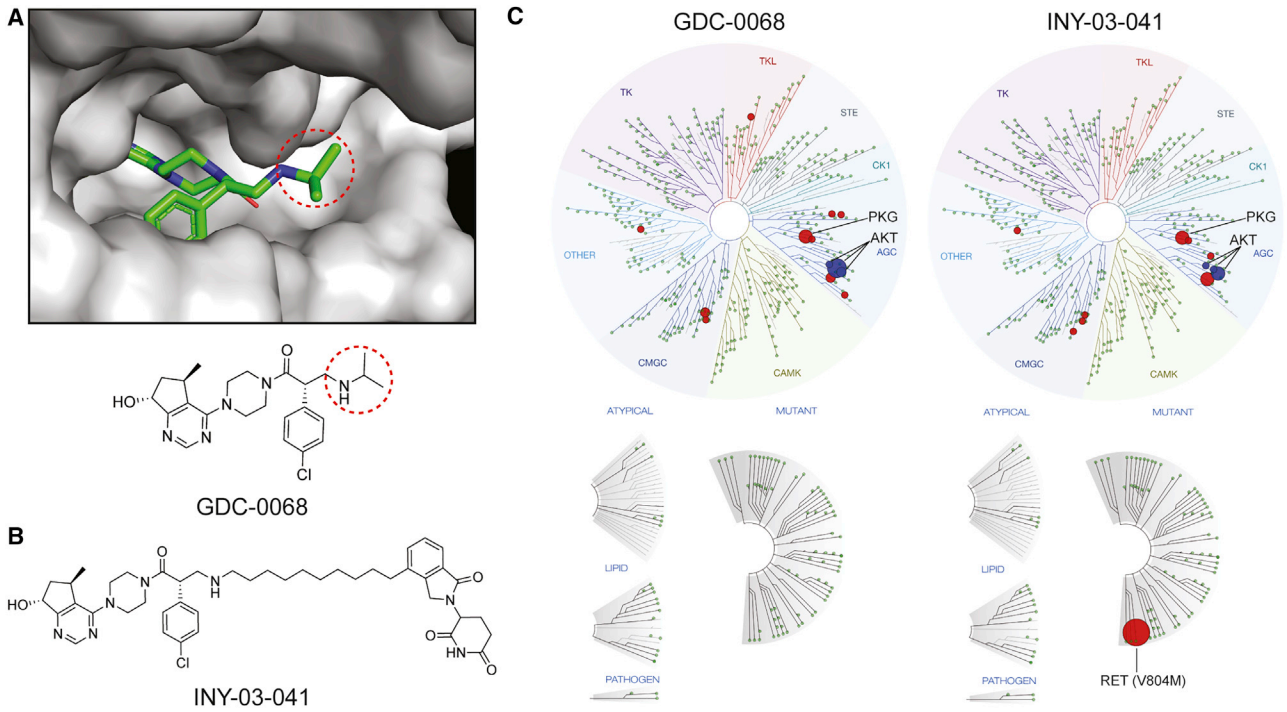

Figure 1. Design and Development of INY-03-041

(A) Co-crystal structure of GDC-0068 (green) bound to AKT1 (gray, PDB: 4EKL) revealing solvent-exposed isopropylamine (circled) where linker was attached.

(B) Chemical structure of INY-03-041.

(C) TREE*spot* visualization of the biochemical kinome selectivity profile of GDC-0068 and INY-03-041 (1 μM). AKT isoforms are highlighted in blue, while all other inhibited kinases are highlighted in red (Table S1).

etiology and progression, AKT is an attractive protein to target for degradation.

Here, we report the development of INY-03-041, a pan-AKT degrader that induces potent degradation of all three AKT isoforms for an extended period of time. Through cell-based assays, we demonstrate that INY-03-041 exhibits more potent and prolonged effects on downstream signaling than GDC-0068, which may explain its enhanced anti-proliferative effects in comparison with the parent catalytic inhibitor. Our data demonstrate that AKT degradation has more durable pharmacological effects than AKT inhibition, which highlights a potentially novel aspect of degrader pharmacology.

RESULTS

Design and Development of the Pan-AKT Degrader INY-03-041

To develop an AKT-targeting heterobifunctional degrader, we designed compounds based on GDC-0068, the most advanced AKT inhibitor in clinical trials (Oliveira et al., 2019). The co-crystal structure of GDC-0068 bound to AKT1 (PDB: 4EKL) revealed that the isopropylamine is solvent exposed, suggesting that the amine could serve as a suitable attachment site for linkers without adversely affecting affinity to AKT (Figure 1A). A ten-hydrocarbon linker was used to conjugate GDC-0068 with lenalidomide to generate INY-03-041 (Figure 1B).

To verify that conjugation of the linker and lenalidomide did not affect the ability of INY-03-041 to bind to AKT, INY-03-041 was tested in a commercially available fluorescence resonance energy transfer-based assay (Invitrogen, Z′-Lyte) for AKT1, AKT2, and AKT3 inhibition (Table S1). INY-03-041 had similar inhibitory activity against AKT1 (half maximal inhibitory concentration [IC_{50}] = 2.0 nM), AKT2 (IC_{50} = 6.8 nM), and AKT3 (IC_{50} = 3.5 nM) as GDC-0068 (IC_{50} values for AKT1, 2, and 3 = 5, 18, and 8 nM, respectively) (Blake et al., 2012), demonstrating that INY-03-041 retained comparable biochemical affinity with all three AKT isoforms as its parent inhibitor. In addition, we evaluated the biochemical selectivity of INY-03-041 against a panel of 468 kinases at 1 μM (KINOMEscan) and observed that INY-03-041 had a similar selectivity profile as GDC-0068 (Figure 1C). Although INY-03-041 scored as a strong binder of RET (V804M) in the KINOMEscan assay, this was confirmed to be a false positive, as its biochemical IC_{50} was determined to be >10,000 nM (Invitrogen, LanthaScreen) (Table S1).

INY-03-041 Is a Potent and Highly Selective Pan-AKT Degrader

After verifying that INY-03-041 engaged AKT biochemically, we sought to characterize its degradation activity in cells. We first chose to evaluate the AKT degrader in the triple-negative breast cancer cell line MDA-MB-468 due to their high expression of all three AKT isoforms. We found that INY-03-041 induced potent degradation of all three AKT isoforms in a dose-dependent manner after a 12-h treatment, with maximal degradation observed between 100 and 250 nM (Figure 2A). At concentrations of 500 nM and greater, we observed diminished AKT degradation,

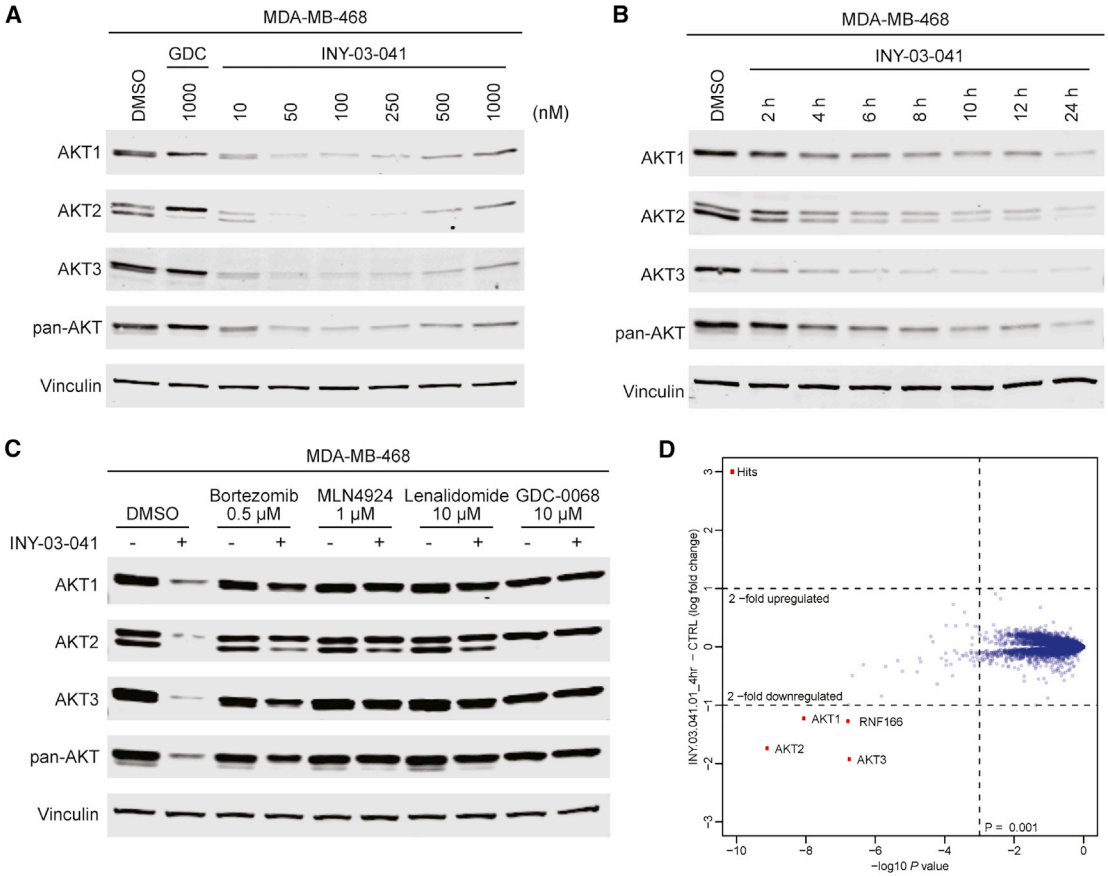

Figure 2. INY-03-041 Induces Potent Degradation of AKT Isoforms Dependent on CRBN, Neddylation, and the Proteasome

(A) Immunoblots for AKT1, AKT2, AKT3, pan-AKT, and Vinculin in MDA-MB-468 cells after 12-h treatment with DMSO, GDC-0068 (GDC), or INY-03-041 at the concentrations indicated (n = 4).

(B) Immunoblots for AKT1, AKT2, AKT3, pan-AKT, and Vinculin in MDA-MB-468 cells after treatment with INY-03-041 (250 nM) at indicated times or DMSO (24 h) (n = 4).

(C) Immunoblots for AKT1, AKT2, AKT3, pan-AKT, and Vinculin after 12-h co-treatment of MDA-MB-468 cells with DMSO, bortezomib (0.5 μM), MLN-4924 (1 μM), lenalidomide (10 μM), or GDC-0068 (10 μM) and either INY-03-041 (250 nM) or DMSO (n = 4).

(D) Scatterplot depicts the change in relative protein abundance of INY-03-041 (250 nM, 4 h)-treated MOLT4 cells compared with DMSO vehicle control-treated cells. Protein abundance measurements were made using tandem mass tag quantitative mass spectrometry and significant changes were assessed by moderated t test as implemented in the limma package (Ritchie et al., 2015). The $\log_2$ fold change ($\log_2$ FC) is shown on the y axis and negative $\log_{10}$ p value ($-\log_{10}$ p value) on the x axis for three independent biological replicates of each treatment.

See also Table S2.

consistent with the hook effect, in which independent engagement of AKT and CRBN by INY-03-041 prevents formation of a productive ternary complex (An and Fu, 2018). Treatment of MDA-MB-468 cells with 250 nM of INY-03-041 over time revealed partial degradation of all AKT isoforms within 4 h and progressive loss of AKT abundance out to 24 h (Figure 2B).

To ensure that INY-03-041-induced AKT degradation was dependent on CRBN, we synthesized INY-03-112, a negative control compound with an N-methylated glutarimide that substantially weakens CRBN binding (Figure S1A) (Brand et al., 2018). INY-03-112 did not induce potent degradation of any AKT isoform (Figure S1B), demonstrating that INY-03-041-induced AKT degradation was CRBN dependent. Furthermore, co-treatment of INY-03-041 with bortezomib, a proteasome inhibitor, or MLN-4924, an NEDD8-activating enzyme inhibitor that prevents neddylation required for the function of cullin RING ligases, such as $CRL4^{CRBN}$ (Soucy et al., 2009), prevented AKT destabilization, indicating that degradation was dependent on the ubiquitin-proteasome system (Figure 2C). Finally, we co-treated INY-03-041 with excess quantities of either GDC-0068 or lenalidomide to compete for binding to AKT or CRBN, respectively, both of which prevented AKT degradation, demonstrating that engagement to both AKT and CRBN is required for INY-03-041-induced AKT degradation (Figure 2C).

To broadly assess degrader selectivity, MOLT4 cells, a cell line that is amenable to proteomics and expresses all three AKT isoforms, were treated with 250 nM of INY-03-041 for 4 h and an unbiased, multiplexed mass spectrometry-based proteomic analysis was performed (Donovan et al., 2018). This analysis identified significant downregulation of all three AKT isoforms, as well as RNF166, a ring-finger protein known to be downregulated by lenalidomide treatment (Figure 2D) (Kronke et al., 2015). Although

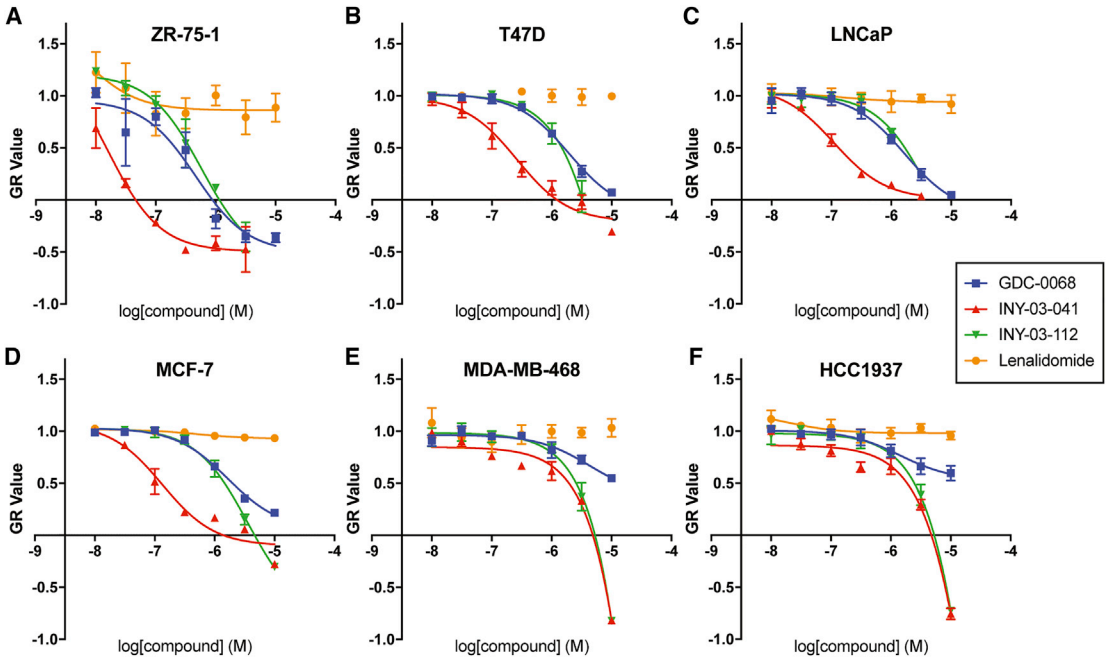

Figure 3. INY-03-041 Induces Enhanced Anti-proliferative Effects Compared with GDC-0068

GR values across concentrations in (A) ZR-75-1, (B) T47D, (C) LNCaP, (D) MCF-7, (E) MDA-MB-468, and (F) HCC1937 cells after 72-h treatment with GDC-0068 (blue), INY-03-041 (red), INY-03-112 (green), and lenalidomide (orange). Error bars represent the standard deviation of three technical replicates.

INY-03-041 exhibited potent *in vitro* inhibition of S6K1 (IC_{50} = 37.3 nM) and PKG1 (IC_{50} = 33.2 nM), both of which are known off-targets of GDC-0068, no downregulation of either kinase was observed in the proteomics (Table S2). Further immunoblot analysis confirmed that INY-03-041 did not induce S6K1 degradation (Figure S1C). Although the time course (Figure 2B) indicates that stronger AKT degradation would be observed at longer time points, it is likely that the results would be confounded by subsequent transcriptional changes caused by AKT degradation.

As CRBN-targeting degraders often destabilize zinc finger proteins, and because we observed IMiD-induced downregulation of RNF166, we examined whether INY-03-041 affected protein abundance levels of Ikaros (IKZF1) and Aiolos (IKZF3), well-established targets of lenalidomide (Kronke et al., 2014). Immunoblot analysis revealed weak IKZF1 and IKZF3 degradation after 24 h of drug treatment, albeit at relatively high concentrations of 500 nM or greater, indicating that INY-03-041 is primarily a selective degrader for AKT (Figure S1C).

INY-03-041 Exhibits Enhanced Anti-proliferative Effects Compared with GDC-0068

As AKT has well-characterized functions in regulating cell proliferation, we next compared the anti-proliferative effects of AKT degradation and inhibition using growth rate inhibition (GR) to account for variation in division rates among cells, as this can confound other drug response metrics, such as IC_{50} values (Hafner et al., 2017). In a panel of cell lines with PI3K pathway mutations that have been reported to be sensitive (ZR-75-1, T47D, LNCaP, and MCF-7) and insensitive (MDA-MB-468 and HCC1937) to AKT inhibition (Table S3) (Lin et al., 2013), we found that INY-03-041 was most potent in ZR-75-1 cells (GR_{50} = 16 nM), with a 14-fold increased potency compared with GDC-0068 (GR_{50} = 229 nM). The anti-proliferative effect of INY-03-041 was degradation dependent, as INY-03-112 was significantly less potent (GR_{50} = 413 nM) than INY-03-041 and had a comparable GR_{50} value with GDC-0068 (Figure 3A; Table S4). Similar trends were seen in the other cell lines sensitive to AKT inhibition, with 8- to 14-fold lower GR_{50} values for INY-03-041 in comparison with GDC-0068 (Figures 3A–3D; Table S4). In addition, lenalidomide, used as a control for RNF166, IKZF1, and IKZF3 degradation, did not have strong anti-proliferative effects, suggesting that the enhanced anti-proliferative effects were due to AKT degradation (Figures 3A–3D).

Although INY-03-041 displayed enhanced anti-proliferative effects compared with GDC-0068 in MDA-MB-468 and HCC1937 cells, there were no apparent differences in GR_{50} values between INY-03-041 and INY-03-112, its non-CRBN binding control (Figures 3E and 3F; Table S4). Thus, the anti-proliferative effects of INY-03-041 in these cell lines were likely due to off-target effects unrelated to AKT degradation that manifest at elevated concentrations of INY-03-041 and INY-03-112. This is consistent with previous studies reporting resistance of MDA-MB-468 and HCC1937 to AKT inhibition (Lin et al., 2013), and indicates that AKT degradation has similar phenotypic effects as AKT inhibition in these cell lines. Overall, the data show that INY-03-041 suppresses proliferation more potently than GDC-0068, and highlight the potential therapeutic value of targeted AKT degradation.

INY-03-041 Suppresses Downstream Signaling More Potently Than GDC-0068

Given the enhanced anti-proliferative effects of INY-03-041 compared with GDC-0068, we sought to compare their effects

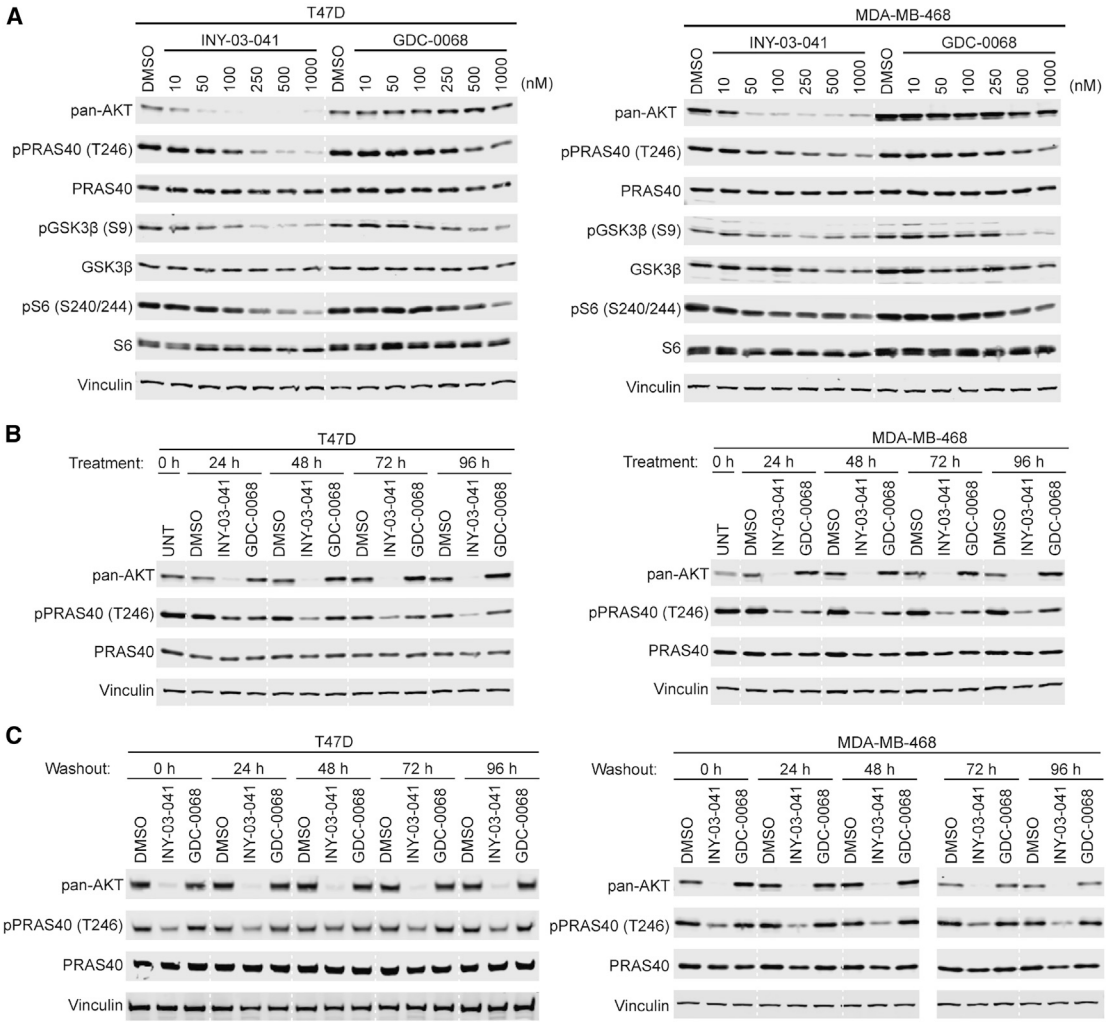

Figure 4. INY-03-041 Exhibits More Potent and Durable Downstream Signaling Effects Than GDC-0068

(A) Immunoblots of pan-AKT, phospho-PRAS40 (T246), total PRAS40, phospho-GSK3β (S9), total GSK3β, phospho-S6 (S240/244), total S6, and Vinculin after treating T47D or MDA-MB-468 cells for 24 h with DMSO, INY-03-041, or GDC-0068 at the concentrations indicated (n = 3).

(B) Immunoblots of pan-AKT, phospho-PRAS40 (T246), total PRAS40, and Vinculin after treatment of T47D or MDA-MB-468 cells with 250 nM of INY-03-041 or GDC-0068 at the time points indicated (n = 3).

(C) Immunoblots of pan-AKT, phospho-PRAS40 (T246), total PRAS40, and Vinculin in T47D or MDA-MB-468 cells treated for 12 h with INY-03-041 or GDC-0068 (250 nM), followed by washout for indicated times (n = 4). Solid vertical white line indicates samples run on separate gels.

on downstream AKT signaling. In T47D cells, which were highly sensitive to INY-03-041 in terms of anti-proliferation, we confirmed that INY-03-041 induced potent AKT degradation, with no detectable levels of all three AKT isoforms observed after a 24-h treatment with 250 nM of INY-03-041 (Figure S2). Moreover, INY-03-041 treatment resulted in robust and dose-dependent inhibition of phosphorylated PRAS40 (pPRAS40) and GSK3β (pGSK3β), well-established direct substrates of AKT (Cross et al., 1995; Wang et al., 2012), as well as S6 (pS6), a downstream marker of AKT activity (Lin et al., 2013) (Figure 4A). Although 250 nM INY-03-041 significantly reduced pPRAS40, pGSK3β, and pS6 levels, doses up to 1 μM of GDC-0068 were required to observe comparable effects (Figure 4A). To test whether these effects were generalizable across distinct cell lines, we also compared the effects of INY-03-041 and GDC-0068 in MDA-MB-468, MOLT4, IGROV1, and PC3 cells (Figures 4A and S3A–S3C). Similar to that observed in T47D cells, INY-03-041 significantly reduced phosphorylation of PRAS40, GSK3β, and S6 at 250 nM, while weaker responses were seen with equivalent doses of GDC-0068 (Figures 4A and S3A–S3C). Although INY-03-041 suppresses downstream AKT signaling more potently than GDC-0068 in a variety of cancer cell lines, longer time points were required for INY-03-041 to display maximal pharmacodynamic effects relative to GDC-0068 (Figures S4A–S4C), consistent with the rate of AKT degradation observed.

Notably, we also found that INY-03-041 promoted sustained destabilization of all three AKT isoforms for at least 96 h after treatment with 250 nM of INY-03-041 in both T47D and MDA-MB-468 cells (Figure 4B). This durable AKT degradation resulted

in sustained inhibition of downstream signaling, as pPRAS40 levels were also significantly reduced for up to 96 h (Figure 4B). By contrast, treatment with an equivalent dose of GDC-0068 not only resulted in less-pronounced inhibition of pPRAS40, but the duration of this effect was also shorter (Figure 4B).

To further characterize the mechanism underlying the extended duration of AKT degradation induced by INY-03-041, we performed compound washout experiments after 12 h of treatment with either 250 nM of INY-03-041 or GDC-0068. We observed no detectable rebound of AKT levels for up to 96 h after washout in INY-03-041-treated cells (Figure 4C), suggesting that the re-synthesis rate of AKT is slow. Consistently, INY-03-041 potently suppressed levels of pPRAS40 for up to 96 h after washout, while washout in GDC-0068-treated cells resulted in rebound of pPRAS40, as would be expected of a reversible inhibitor (Figure 4C). Taken together, our data suggest that INY-03-041-mediated AKT degradation resulted in more potent and durable pharmacological effects than AKT inhibition.

DISCUSSION

Heterobifunctional degraders have garnered attention recently due to potential advantages over traditional small-molecule inhibitors, including their ability to target proteins deemed undruggable through the use of non-functional ligands (Farnaby et al., 2019; Silva et al., 2019) and to achieve selectivity with promiscuous ligands (Nowak et al., 2018). However, one advantage of degraders that has not been fully investigated is their potential to exert long-lasting pharmacological effects. Because degraders deplete abundance of a targeted protein, short-term drug exposure may deliver sustained pharmacological effects, uncoupling pharmacodynamics from pharmacokinetics. This distinction may be more apparent for proteins with slow re-synthesis rates, as longer periods of time may be required for protein levels to recover and re-establish physiological signaling.

Consistent with the long-reported half-life for AKT (Basso et al., 2002), INY-03-041 destabilized all three AKT isoforms and diminished downstream signaling effects for up to 96 h, even after compound washout. This durable and prolonged pharmacodynamic effect, which was significantly greater than that of the parent AKT inhibitor GDC-0068, may explain, at least in part, the more potent anti-proliferative effects of INY-03-041. To the best of our knowledge, this is the first example of a small-molecule degrader that sustains knockdown and downstream signaling effects for such an extended period of time, and exemplifies a distinguishing feature of degrader pharmacology.

Although several ATP-competitive and allosteric AKT inhibitors have entered clinical trials, dose-limiting toxicities or lack of clinical efficacy have hindered their progress (Jansen et al., 2016). Moreover, AKT has been reported to have kinase-independent functions (Vivanco et al., 2014) that would reduce efficacy of small-molecule inhibitors, and resistance to AKT inhibitors can arise in some contexts due to upregulation of AKT3 (Stottrup et al., 2016). As degraders have been reported to abrogate kinase-independent functions (Cromm et al., 2018) and overcome inhibitor-induced compensatory upregulation of target proteins (Cai et al., 2012; Han et al., 2019), targeted AKT degradation may be a promising alternative approach for therapeutic intervention in cancers with PI3K/AKT pathway alterations. Although our data suggest that AKT degraders can induce more potent and durable downstream effects than AKT inhibitors, further optimization, particularly of the pharmacokinetic properties of the large heterobifunctional degrader molecules will be necessary. In addition, reported on-target toxicities with AKT inhibitors (Jansen et al., 2016) suggest that more potent degraders may have a narrow therapeutic window, further necessitating the need to investigate the therapeutic viability of targeted AKT degradation.

Our data also support the value of INY-03-041 as a chemical probe for studying the acute biological effects of pan-AKT depletion. Existing methods for inducing AKT1, AKT2, and AKT3 depletion in cells have relied on CRISPR knockout or repression, doxycycline-inducible small-hairpin RNAs, or transient transfection with small interfering RNA, all of which require relatively long incubation periods (Degtyarev et al., 2008; Koseoglu et al., 2007). This not only prevents assessment of acute biological changes resulting from loss of AKT, but also may allow reprogramming and compensation of cellular networks. By contrast, INY-03-041 induces rapid degradation of all three AKT isoforms, thereby permitting the investigation of the phenotypes of acute pan-AKT depletion. Therefore, INY-03-041 will be a useful chemical tool to explore AKT biology inaccessible with current strategies.

SIGNIFICANCE

Although many small-molecule AKT inhibitors have been developed, here we demonstrate an alternative approach to targeting AKT by inducing its degradation, which resulted in distinct pharmacological effects. INY-03-041, a heterobifunctional degrader, promoted rapid and highly selective degradation of all three AKT isoforms and had more potent anti-proliferative effects than GDC-0068, the most clinically advanced AKT inhibitor. More importantly, INY-03-041-induced degradation of AKT and the ensuing suppression of downstream signaling was sustained for several days. Our work showcases the extended pharmacodynamic effects of degraders, and presents INY-03-041 as a tool to study acute changes to the AKT signaling network after rapid AKT degradation.

STAR★METHODS

Detailed methods are provided in the online version of this paper and include the following:

- KEY RESOURCES TABLE
- LEAD CONTACT AND MATERIALS AVAILABILITY
- EXPERIMENTAL MODEL AND SUBJECT DETAILS
- METHODS DETAILS
  - Drug Treatment Experiments
  - Immunoblotting
  - Growth Rate Assay and Analysis
  - In Vitro Kinase Assays
  - TMT LC-MS Sample Preparation
  - LC-MS Data Analysis
  - Chemistry Synthetic Scheme

SUPPLEMENTAL INFORMATION

Supplemental Information can be found online at https://doi.org/10.1016/j.chembiol.2019.11.014.

ACKNOWLEDGMENTS

We would like to thank Eric Wang and Milka Kostic for helpful comments on the manuscript. We would also like to thank Caitlin Mills and Kartik Subramanian (Laboratory for Systems Pharmacology at Harvard Medical School) for their help with proliferation data collection and analysis. This work was supported by the Training Grant in Chemical Biology (NIH 7 T32 GM095450-07, to I.Y.), the Training Grant in Pharmacological Sciences (NIH 1 T32 GM132089-01, to I.Y.), the National Science Foundation Graduate Research Fellowship Program (DGE1745303, to E.C.E.), the NIH 1R01 CA218278-01A1 (to E.S.F. and N.S.G.) and the Ludwig Center at Harvard (to E.C.E. and A.T.).

AUTHOR CONTRIBUTIONS

A.T. and N.S.G. conceived the study. I.Y. designed and synthesized the compounds. E.C.E. and I.Y. designed and conducted the biological profiling of the degraders. K.A.D. and N.A.E. performed the proteomics. I.Y and E.C.E wrote the manuscript, with guidance from E.S.F., N.S.G., and A.T. All authors gave feedback on the manuscript.

DECLARATION OF INTERESTS

A.T. is a consultant for Oncologie, Inc. N.S.G. is a scientific founder and member of the Scientific Advisory Board (SAB) of C4 Therapeutics, Syros, Soltego, B2S, Gatekeeper, and Petra Pharmaceuticals, and has received research funding from Novartis, Astellas, Taiho, and Deerfield. E.S.F. is a founder and/or member of the SAB, and equity holder of C4 Therapeutics and Civetta Therapeutics, and a consultant to Novartis, AbbVie, and Pfizer. The Fischer lab receives research funding from Novartis, Deerfield, and Astellas. I.Y., E.C.E., K.A.D., E.S.F., A.T., and N.S.G. are inventors on a patent application related to the AKT degraders described in this manuscript.

Received: September 12, 2019
Revised: October 28, 2019
Accepted: November 25, 2019
Published: December 16, 2019

SUPPORTING CITATIONS

The following references appear in the Supplemental Information: Meric-Bernstam et al., 2012; Vlietstra et al., 1998.

REFERENCES

An, J., Ponthier, C.M., Sack, R., Seebacher, J., Stadler, M.B., Donovan, K.A., and Fischer, E.S. (2017). pSILAC mass spectrometry reveals ZFP91 as IMiD-dependent substrate of the CRL4CRBN ubiquitin ligase. Nat. Commun. *8*, 15398.

An, S., and Fu, L. (2018). Small-molecule PROTACs: an emerging and promising approach for the development of targeted therapy drugs. EBioMedicine *36*, 553–562.

Basso, A.D., Solit, D.B., Chiosis, G., Giri, B., Tsichlis, P., and Rosen, N. (2002). Akt forms an intracellular complex with heat shock protein 90 (Hsp90) and Cdc37 and is destabilized by inhibitors of Hsp90 function. J. Biol. Chem. *277*, 39858–39866.

Blake, J.F., Xu, R., Bencsik, J.R., Xiao, D., Kallan, N.C., Schlachter, S., Mitchell, I.S., Spencer, K.L., Banka, A.L., Wallace, E.M., et al. (2012). Discovery and preclinical pharmacology of a selective ATP-competitive Akt inhibitor (GDC-0068) for the treatment of human tumors. J. Med. Chem. *55*, 8110–8127.

Brand, M., Jiang, B., Bauer, S., Donovan, K.A., Liang, Y., Wang, E.S., Nowak, R.P., Yuan, J.C., Zhang, T., Kwiatkowski, N., et al. (2018). Homolog-selective degradation as a strategy to probe the function of CDK6 in AML. Cell Chem Biol. *26*, 300–306.e9.

Brown, J.S., and Banerji, U. (2017). Maximising the potential of AKT inhibitors as anti-cancer treatments. Pharmacol. Ther. *172*, 101–115.

Cai, J., Cai, L.Q., Hong, Y., and Zhu, Y.S. (2012). Functional characterisation of a natural androgen receptor missense mutation (N771H) causing human androgen insensitivity syndrome. Andrologia *44* (*Suppl 1*), 523–529.

Cantley, L.C., and Neel, B.G. (1999). New insights into tumor suppression: PTEN suppresses tumor formation by restraining the phosphoinositide 3-kinase/AKT pathway. Proc. Natl. Acad. Sci. U S A *96*, 4240–4245.

Churcher, I. (2018). Protac-induced protein degradation in drug discovery: breaking the rules or just making new ones? J. Med. Chem. *61*, 444–452.

Cromm, P.M., Samarasinghe, K.T.G., Hines, J., and Crews, C.M. (2018). Addressing kinase-independent functions of Fak via PROTAC-mediated degradation. J. Am. Chem. Soc. *140*, 17019–17026.

Cross, D.A., Alessi, D.R., Cohen, P., Andjelkovich, M., and Hemmings, B.A. (1995). Inhibition of glycogen synthase kinase-3 by insulin mediated by protein kinase B. Nature *378*, 785–789.

Degtyarev, M., De Maziere, A., Orr, C., Lin, J., Lee, B.B., Tien, J.Y., Prior, W.W., van Dijk, S., Wu, H., Gray, D.C., et al. (2008). Akt inhibition promotes autophagy and sensitizes PTEN-null tumors to lysosomotropic agents. J. Cell Biol. *183*, 101–116.

Do, K., Speranza, G., Bishop, R., Khin, S., Rubinstein, L., Kinders, R.J., Datiles, M., Eugeni, M., Lam, M.H., Doyle, L.A., et al. (2015). Biomarker-driven phase 2 study of MK-2206 and selumetinib (AZD6244, ARRY-142886) in patients with colorectal cancer. Invest. New Drugs *33*, 720–728.

Dobrovolsky, D., Wang, E.S., Morrow, S., Leahy, C., Faust, T., Nowak, R.P., Donovan, K.A., Yang, G., Li, Z., Fischer, E.S., et al. (2018). Bruton's tyrosine kinase degradation as a therapeutic strategy for cancer. Blood *133*, 952–961.

Donovan, K.A., An, J., Nowak, R.P., Yuan, J.C., Fink, E.C., Berry, B.C., Ebert, B.L., and Fischer, E.S. (2018). Thalidomide promotes degradation of SALL4, a transcription factor implicated in Duane Radial Ray syndrome. Elife *7*, https://doi.org/10.7554/eLife.38430.

Farnaby, W., Koegl, M., Roy, M.J., Whitworth, C., Diers, E., Trainor, N., Zollman, D., Steurer, S., Karolyi-Oezguer, J., Riedmueller, C., et al. (2019). BAF complex vulnerabilities in cancer demonstrated via structure-based PROTAC design. Nat. Chem. Biol. *15*, 672–680.

Fruman, D.A., Chiu, H., Hopkins, B.D., Bagrodia, S., Cantley, L.C., and Abraham, R.T. (2017). The PI3K pathway in human disease. Cell *170*, 605–635.

Hafner, M., Heiser, L.M., Williams, E.H., Niepel, M., Wang, N.J., Korkola, J.E., Gray, J.W., and Sorger, P.K. (2017). Quantification of sensitivity and resistance of breast cancer cell lines to anti-cancer drugs using GR metrics. Sci. Data *4*, 170166.

Han, X., Wang, C., Qin, C., Xiang, W., Fernandez-Salas, E., Yang, C.Y., Wang, M., Zhao, L., Xu, T., Chinnaswamy, K., et al. (2019). Discovery of ARD-69 as a highly potent proteolysis targeting chimera (PROTAC) degrader of androgen receptor (AR) for the treatment of prostate cancer. J. Med. Chem. *62*, 941–964.

Huck, B.R., and Mochalkin, I. (2017). Recent progress towards clinically relevant ATP-competitive Akt inhibitors. Bioorg. Med. Chem. Lett. *27*, 2838–2848.

Jansen, V.M., Mayer, I.A., and Arteaga, C.L. (2016). Is there a future for AKT inhibitors in the treatment of cancer? Clin. Cancer Res. *22*, 2599–2601.

Keppler-Noreuil, K.M., Sapp, J.C., Lindhurst, M.J., Darling, T.N., Burton-Akright, J., Bagheri, M., Dombi, E., Gruber, A., Jarosinski, P.F., Martin, S., et al. (2019). Pharmacodynamic study of miransertib in individuals with Proteus syndrome. Am. J. Hum. Genet. *104*, 484–491.

Koseoglu, S., Lu, Z., Kumar, C., Kirschmeier, P., and Zou, J. (2007). AKT1, AKT2 and AKT3-dependent cell survival is cell line-specific and knockdown of all three isoforms selectively induces apoptosis in 20 human tumor cell lines. Cancer Biol. Ther. *6*, 755–762.

Kronke, J., Fink, E.C., Hollenbach, P.W., MacBeth, K.J., Hurst, S.N., Udeshi, N.D., Chamberlain, P.P., Mani, D.R., Man, H.W., Gandhi, A.K., et al. (2015). Lenalidomide induces ubiquitination and degradation of CK1alpha in del(5q) MDS. Nature *523*, 183–188.

Kronke, J., Hurst, S.N., and Ebert, B.L. (2014). Lenalidomide induces degradation of IKZF1 and IKZF3. Oncoimmunology *3*, e941742.

Lin, J., Sampath, D., Nannini, M.A., Lee, B.B., Degtyarev, M., Oeh, J., Savage, H., Guan, Z., Hong, R., Kassees, R., et al. (2013). Targeting activated Akt with GDC-0068, a novel selective Akt inhibitor that is efficacious in multiple tumor models. Clin. Cancer Res. *19*, 1760–1772.

Manning, B.D., and Toker, A. (2017). AKT/PKB signaling: navigating the network. Cell *169*, 381–405.

McAlister, G.C., Nusinow, D.P., Jedrychowski, M.P., Wuhr, M., Huttlin, E.L., Erickson, B.K., Rad, R., Haas, W., and Gygi, S.P. (2014). MultiNotch MS3 enables accurate, sensitive, and multiplexed detection of differential expression across cancer cell line proteomes. Anal Chem. *86*, 7150–7158.

Meric-Bernstam, F., Akcakanat, A., Chen, H., Do, K.A., Sangai, T., Adkins, F., Gonzalez-Angulo, A.M., Rashid, A., Crosby, K., Dong, M., et al. (2012). PIK3CA/PTEN mutations and Akt activation as markers of sensitivity to allosteric mTOR inhibitors. Clin. Cancer Res. *18*, 1777–1789.

Nowak, R.P., DeAngelo, S.L., Buckley, D., He, Z., Donovan, K.A., An, J., Safaee, N., Jedrychowski, M.P., Ponthier, C.M., Ishoey, M., et al. (2018). Plasticity in binding confers selectivity in ligand-induced protein degradation. Nat. Chem. Biol. *14*, 706–714.

Oliveira, M., Saura, C., Nuciforo, P., Calvo, I., Andersen, J., Passos-Coelho, J.L., Gil Gil, M., Bermejo, B., Patt, D.A., Ciruelos, E., et al. (2019). FAIRLANE, a double-blind placebo-controlled randomized phase II trial of neoadjuvant ipatasertib plus paclitaxel for early triple-negative breast cancer. Ann. Oncol. https://doi.org/10.1093/annonc/mdz177.

Olson, C.M., Jiang, B., Erb, M.A., Liang, Y., Doctor, Z.M., Zhang, Z., Zhang, T., Kwiatkowski, N., Boukhali, M., Green, J.L., et al. (2018). Pharmacological perturbation of CDK9 using selective CDK9 inhibition or degradation. Nat. Chem. Biol. *14*, 163–170.

Ritchie, M.E., Phipson, B., Wu, D., Hu, Y., Law, C.W., Shi, W., and Smyth, G.K. (2015). Limma powers differential expression analyses for RNA-sequencing and microarray studies. Nucleic Acids Res. *43*, e47.

Shayesteh, L., Lu, Y., Kuo, W.L., Baldocchi, R., Godfrey, T., Collins, C., Pinkel, D., Powell, B., Mills, G.B., and Gray, J.W. (1999). PIK3CA is implicated as an oncogene in ovarian cancer. Nat. Genet. *21*, 99–102.

Silva, M.C., Ferguson, F.M., Cai, Q., Donovan, K.A., Nandi, G., Patnaik, D., Zhang, T., Huang, H.T., Lucente, D.E., Dickerson, B.C., et al. (2019). Targeted degradation of aberrant tau in frontotemporal dementia patient-derived neuronal cell models. Elife *8*, https://doi.org/10.7554/eLife.45457.

Soucy, T.A., Smith, P.G., and Rolfe, M. (2009). Targeting NEDD8-activated cullin-RING ligases for the treatment of cancer. Clin. Cancer Res. *15*, 3912–3916.

Stottrup, C., Tsang, T., and Chin, Y.R. (2016). Upregulation of AKT3 confers resistance to the AKT inhibitor MK2206 in breast cancer. Mol. Cancer Ther. *15*, 1964–1974.

Team, R.C. (2013). R: A Language and Environment for Statistical Computing (R Foundation for Statistical Computing).

Toker, A. (2012). Achieving specificity in Akt signaling in cancer. Adv. Biol. Regul. *52*, 78–87.

Turner, N.C., Alarcon, E., Armstrong, A.C., Philco, M., Lopez Chuken, Y.A., Sablin, M.P., Tamura, K., Gomez Villanueva, A., Perez-Fidalgo, J.A., Cheung, S.Y.A., et al. (2019). BEECH: a dose-finding run-in followed by a randomised phase II study assessing the efficacy of AKT inhibitor capivasertib (AZD5363) combined with paclitaxel in patients with estrogen receptor-positive advanced or metastatic breast cancer, and in a PIK3CA mutant sub-population. Ann. Oncol. *30*, 774–780.

Uhlenbrock, N., Smith, S., Weisner, J., Landel, I., Lindemann, M., Le, T.A., Hardick, J., Gontla, R., Scheinpflug, R., Czodrowski, P., et al. (2019). Structural and chemical insights into the covalent-allosteric inhibition of the protein kinase Akt. Chem. Sci. *10*, 3573–3585.

Vivanco, I., Chen, Z.C., Tanos, B., Oldrini, B., Hsieh, W.Y., Yannuzzi, N., Campos, C., and Mellinghoff, I.K. (2014). A kinase-independent function of AKT promotes cancer cell survival. Elife *3*, https://doi.org/10.7554/eLife.03751.

Vlietstra, R.J., van Alewijk, D.C., Hermans, K.G., van Steenbrugge, G.J., and Trapman, J. (1998). Frequent inactivation of PTEN in prostate cancer cell lines and xenografts. Cancer Res. *58*, 2720–2723.

Wang, H., Zhang, Q., Wen, Q., Zheng, Y., Lazarovici, P., Jiang, H., Lin, J., and Zheng, W. (2012). Proline-rich Akt substrate of 40kDa (PRAS40): a novel downstream target of PI3k/Akt signaling pathway. Cell Signal. *24*, 17–24.

Winter, G.E., Buckley, D.L., Paulk, J., Roberts, J.M., Souza, A., Dhe-Paganon, S., and Bradner, J.E. (2015). DRUG DEVELOPMENT. Phthalimide conjugation as a strategy for in vivo target protein degradation. Science *348*, 1376–1381.

Zhou, B., Hu, J., Xu, F., Chen, Z., Bai, L., Fernandez-Salas, E., Lin, M., Liu, L., Yang, C.Y., Zhao, Y., et al. (2018). Discovery of a small-molecule degrader of bromodomain and extra-terminal (BET) proteins with picomolar cellular potencies and capable of achieving tumor regression. J. Med. Chem. *61*, 462–481.

STAR★METHODS

KEY RESOURCES TABLE

REAGENT or RESOURCE	SOURCE	IDENTIFIER
Antibodies		
Rabbit monoclonal anti AKT1	Cell Signaling Technology	Cat# 2938; RRID: AB_915788
Rabbit monoclonal anti AKT2	Cell Signaling Technology	Cat# 3063; RRID: AB_2225186
Mouse monoclonal anti AKT3	Cell Signaling Technology	Cat# 8018; RRID: AB_10859371
Rabbit monoclonal anti AKT (pan)	Cell Signaling Technology	Cat# 4691; RRID: AB_915783
Mouse monoclonal anti AKT (pan)	Cell Signaling Technology	Cat# 2920; RRID: AB_1147620
Rabbit monoclonal anti Phospho-PRAS40 (T246)	Cell Signaling Technology	Cat# 2997; RRID: AB_2258110
Rabbit monoclonal anti PRAS40	Cell Signaling Technology	Cat# 2691; RRID: AB_2225033
Rabbit monoclonal anti GSK3β	Cell Signaling Technology	Cat# 9315; RRID: AB_490890
Rabbit polyclonal anti Phospho-GSK3β (S9)	Cell Signaling Technology	Cat# 9336; RRID: AB_331405
Rabbit monoclonal anti S6 Ribosomal Protein	Cell Signaling Technology	Cat# 2217; RRID: AB_331355
Rabbit polyclonal anti Phospho-S6 Ribosomal Protein (S240/244)	Cell Signaling Technology	Cat# 2215; RRID: AB_331682
Rabbit monoclonal anti Phospho-S6 Ribosomal Protein (S240/244)	Cell Signaling Technology	Cat# 5364; RRID: AB_1069423
Rabbit monoclonal anti Vinculin	Cell Signaling Technology	Cat# 13901; RRID: AB_2728768
Rabbit monoclonal anti p70S6 Kinase	Cell Signaling Technology	Cat# 2708; RRID: AB_390722
Rabbit monoclonal anti Ikaros	Cell Signaling Technology	Cat# 14859; RRID: AB_2744523
Rabbit monoclonal anti Aiolos	Cell Signaling Technology	Cat# 15103; RRID: AB_2744524
Rabbit monoclonal anti β-actin	Cell Signaling Technology	Cat# 4970; RRID: AB_2223172
Chemicals, Peptides, and Recombinant Proteins		
DMSO	Fisher	Cat# BP231-100
Bortezomib (PS-341)	Cayman Chemical	Cat# 10008822
Pevonedistat (MLN4924)	Selleckchem	Cat# S7109
GDC-0068	Selleckchem	Cat# S2808
Lenalidomide	Sigma Aldrich	Cat# 901558
Penicillin Streptomycin	Thermo Fisher Scientific	Cat# 15140122
RPMI Medium	Wisent Bioproducts	Cat# 350000CL
DMEM Medium	Thermo Fisher Scientific	Cat# 11965118
LIVE/DEAD Far Red	Thermo Fisher Scientific	Cat# L34974
INY-03-041	This study	N/A
INY-03-112	This study	N/A

(*Continued on next page*)

Continued

REAGENT or RESOURCE	SOURCE	IDENTIFIER
Critical Commercial Assays		
Z' Lyte (AKT1)	Invitrogen	Assay ID 247
Z' Lyte (AKT2)	Invitrogen	Assay ID 250
Z' Lyte (AKT3)	Invitrogen	Assay ID 253
Z' Lyte (PKG1)	Invitrogen	Assay ID 757
Z' Lyte (S6K1)	Invitrogen	Assay ID 810
Z' Lyte (PKN1)	Invitrogen	Assay ID 703
Z' Lyte (βMSK2)	Invitrogen	Assay ID 801
Z' Lyte (Haspin)	Invitrogen	Assay ID 1115
Lanthascreen (RET (V804M))	Invitrogen	Assay ID 1847
Deposited Data		
INY-03-041 Proteomics in MOLT4 cells	This study	Pride: PXD015207
Experimental Models: Cell Lines		
MOLT4	ATCC	CRL-1582; RRID: CVCL_0013
Jurkat	ATCC	TIB-152; RRID: CVCL_0367
ZR-75-1	ATCC	CRL-1500; RRID: CVCL_0588
LNCaP	Steven P. Balk's Lab	N/A
T47D	ATCC	HTB-133; RRID: CVCL_0553
MCF7	ATCC	HTB-22; RRID:CVCL_0031
MDA-MB-468	ATCC	HTB-132; RRID: CVCL_0419
HCC1937	ATCC	CRL-2336; RRID: CVCL_0290
IGROV1	Panagiotis A. Konstantinopoulos's Lab	N/A
PC3	Jarrod A. Marto's Lab	N/A
Software and Algorithms		
GraphPad Prism	GraphPad Software, Inc.	www.graphpad.com/
Columbus image storage and analysis	PerkinElmer Informatics	http://www.perkinelmer.com/product/image-data-storage-and-analysis-system-columbus
Adobe Illustrator	Adobe Creative Cloud	https://www.adobe.com/creativecloud.html
Proteome Discoverer 2.2	Thermo Fisher Scientific	https://www.thermofisher.com/order/catalog/product/OPTON-30795
R Framework	Team RCR: A Language and Environment for Statistical Computing	http://www.R-project.org/
Python 3.7.3	Python Software Foundation	https://www.python.org/

LEAD CONTACT AND MATERIALS AVAILABILITY

Further information and requests for resources and reagents should be directed to and will be fulfilled by the Lead Contact, Alex Toker (atoker@bidmc.harvard.edu). Requested compounds will be provided following completion of an MTA.

EXPERIMENTAL MODEL AND SUBJECT DETAILS

MOLT4 (male, CVCL_0013), Jurkat (male, CVCL_0065), ZR-75-1 (female, CVCL_0588), LNCaP (male, VCL_0395), T47D (female, CVCL_0553), MCF-7 (female, CVCL_0031) , MDA-MB-468 (female, CVCL_0419) , and HCC1937 (female, CVCL_0290) cells were cultured in RPMI media (Wisent Bioproducts) supplemented with 10% heat inactivated fetal bovine serum (Thermo Fisher Scientific) and 100U/mL Penicillin-Streptomycin (Gibco) at 37°C in the presence of 5% CO_2. IGROV1 (female, CVCL_1304) and PC3 (male, CVCL_0035) cells were cultured in DMEM media (Gibco) supplemented with 10% heat inactivated fetal bovine serum (Thermo Fisher Scientific) and 100U/mL Penicillin-Streptomycin (Gibco) at 37°C in the presence of 5% CO_2.

METHODS DETAILS

Drug Treatment Experiments

Cells were plated at 250,000 cells per mL (MDA-MB-468, MOLT4, IGROV1, PC3, and Jurkat) or 200,000 cells per mL (T47D) in 2 mL per well of RPMI or DMEM media with 10% serum in 6-well treated tissue culture plates (Greiner, Cat # TCG-657160) or 60 mm treated tissue culture plates (Corning, Cat # 430166) and incubated overnight. The next day, cells were treated with the indicated compounds at the appropriate concentration and protein lysates were harvested at the times specified.

Immunoblotting

Cells were washed once in 1x PBS then lysed in RIPA buffer (150 mM Tris-HCl, 150 mM NaCl, 0.5% (w/v) sodium deoxycholate, 1% (v/v) NP-40, pH 7.5) containing 0.1% (w/v) sodium dodecyl sulfate, 1 mM sodium pyrophosphate, 20 mM sodium fluoride, 50 nM calyculin, and 0.5% (v/v) protease inhibitor cocktail (Sigma-Aldrich®) for 15 minutes. Cell extracts were precleared by centrifugation at 14,000 rpm for 10 minutes at 4°C. The Bio-Rad DC protein assay was used to assess protein concentration, and sample concentration was normalized using SDS sample buffer. Lysates were resolved on acrylamide gels by SDS-polyacrylamide gel electrophoresis and electrophoretically transferred to nitrocellulose membrane (BioRad) at 100 volts for 90 minutes. Membranes were blocked in 5% (w/v) nonfat dry milk in tris-buffered saline (TBS) buffer for 1 hour then incubated with specific primary antibodies diluted in 5% (w/v) nonfat dry milk in TBS-T (TBS with 0.05% Tween-20) at 4°C overnight, shaking. The next day, membranes were washed with TBS-T then incubated for 1 hour at room temperature with fluorophore-conjugated secondary antibodies (LI-COR Biosciences). The membrane was washed again with TBS-T then imaged with a LI-COR Odyssey CLx Imaging System (LI-COR Biosciences).

Growth Rate Assay and Analysis

Cell lines were plated at densities ranging from 500 to 2000 cells per well in a 384-well plate using a Matrix WellMate Reagent Dispenser (Thermo Fisher) and allowed 24 hours to adhere to plate prior to treatment. A D300 Digital Dispenser (Hewlett-Packard) was used to treat cells with dilution series of compounds as indicated. At the time of treatment and after 72 hours of treatment, cells were stained and fixed for subsequent analysis. Cells were stained with LIVE/DEAD Far Red Dead Cell Stain (LDR) (Thermo Fisher Scientific) at 1:2000 for 1 hour at 37°C. Cells were fixed for 30 minutes at room temperature in 4% formaldehyde (Sigma Aldrich) then permeabilized with 0.5% Triton X-100 in PBS. Cells were blocked for 1 hour using Odyssey Blocking Buffer (LI-COR Biosciences) and stained overnight at 4°C with 2 μg/ml Hoechst 33342 (Sigma Aldrich). An Operetta microscope was used to image fixed cells, and data was stored and analyzed using Columbus software (PerkinElmer). Nuclei were segmented by Hoechst signal using the Columbus system (Perkin Elmer). The average LDR and Hoechst intensities were determined within the nuclear area. Dead cells were classified by LDR signal. Experiments were performed in technical triplicate.

In Vitro Kinase Assays

Z'-LYTE assays were conducted for AKT1, AKT2, AKT3, PKG1, S6K1, PKN1, ßMSK2, and Haspin at Life Technologies in a 10-point dose response using Km ATP concentrations. LanthaScreen assays were conducted for RET (V804M) in a 10-point dose response at Life Technologies.

TMT LC-MS Sample Preparation

MOLT4 cells were treated with DMSO, 250 nM INY-03-041-01 for 4 hours in biological triplicates. Cells were harvested by centrifugation. Lysis buffer (8 M Urea, 50 mM NaCl, 50 mM 4-(2hydroxyethyl)-1-piperazineethanesulfonic acid (EPPS) pH 8.5, 1x Roche protease inhibitor and 1x Roche PhosphoStop was added to the cell pellets and cells were homogenized by 20 passes through a 21 gauge (1.25 in. long) needle to achieve a cell lysate with a protein concentration between 0.5 – 4 mg mL^{-1}. The homogenized sample was clarified by centrifugation at 20,000 x g for 10 minutes at 4°C. A Bradford assay was used to determine the final protein concentration in the cell lysate. 200 μg protein for each sample were reduced and alkylated as previously described (An et al., 2017). Proteins were precipitated using methanol/chloroform. In brief, four volumes of methanol were added to the cell lysate, followed by one volume of chloroform, and finally three volumes of water. The mixture was vortexed and centrifuged at 14,000 x g for 5 minutes

to separate the chloroform phase from the aqueous phase. The precipitated protein was washed with three volumes of methanol, centrifuged at 14,000 x g for 5 min, and the resulting washed precipitated protein was allowed to air dry. Precipitated protein was resuspended in 4 M Urea, 50 mM HEPES pH 7.4, followed by dilution to 1 M urea with the addition of 200 mM EPPS pH 8 for digestion with LysC (1:50; enzyme:protein) for 12 hours at RT. The LysC digestion was diluted to 0.5 M Urea, 200 mM EPPS pH 8 and then digested with trypsin (1:50; enzyme:protein) for 6 hours at 37°C. Tandem mass tag (TMT) reagents (Thermo Fisher Scientific) were dissolved in anhydrous acetonitrile (ACN) according to manufacturer's instructions. Anhydrous ACN was added to each peptide sample to a final concentration of 30% v/v, and labeling was induced with the addition of TMT reagent to each sample at a ratio of 1:4 peptide:TMT label. The 11-plex labeling reactions were performed for 1.5 hours at RT and the reaction quenched by the addition of 0.3% hydroxylamine for 15 minutes at RT. The sample channels were combined at a 1:1:1:1:1:1:1:1:1:1:1 ratio, desalted using C_{18} solid phase extraction cartridges (Waters) and analyzed by LC-MS for channel ratio comparison. Samples were then combined using the adjusted volumes determined in the channel ratio analysis and dried down in a speed vacuum. The combined sample was then resuspended in 1% formic acid and acidified (pH 2–3) before being subjected to desalting with C18 SPE (Sep-Pak, Waters). Samples were then offline fractionated into 96 fractions by high pH reverse-phase HPLC (Agilent LC1260) through an aeris peptide xb-c18 column (phenomenex) with mobile phase A containing 5% acetonitrile and 10 mM NH_4HCO_3 in LC-MS grade H_2O, and mobile phase B containing 90% acetonitrile and 10 mM NH_4HCO_3 in LC-MS grade H_2O (both pH 8.0). The 96 resulting fractions were then pooled in a non-continuous manner into 24 fractions and every fraction was used for subsequent mass spectrometry analysis.

Data were collected using an Orbitrap Fusion Lumos mass spectrometer (Thermo Fisher Scientific, San Jose, CA, USA) coupled with a Proxeon EASY-nLC 1200 LC pump (Thermo Fisher Scientific). Peptides were separated on a 50 cm and 75 μm inner diameter Easyspray column (ES803a, Thermo Fisher Scientific). Peptides were separated using a 190 minute gradient of 6 – 27% acetonitrile in 1.0% formic acid with a flow rate of 300 nL/min.

Each analysis used an MS^3-based TMT method as described previously (McAlister et al., 2014). The data were acquired using a mass range of *m/z* 340 – 1350, resolution 120,000, AGC target 5 x 10^5, maximum injection time 100 ms, dynamic exclusion of 120 seconds for the peptide measurements in the Orbitrap. Data dependent MS^2 spectra were acquired in the ion trap with a normalized collision energy (NCE) set at 35%, AGC target set to 1.8 x 10^4 and a maximum injection time of 120 ms. MS^3 scans were acquired in the Orbitrap with a HCD collision energy set to 55%, AGC target set to 2 x 10^5, maximum injection time of 150 ms, resolution at 50,000 and with a maximum synchronous precursor selection (SPS) precursors set to 10.

LC-MS Data Analysis

Proteome Discoverer 2.2 (Thermo Fisher) was used for .RAW file processing and controlling peptide and protein level false discovery rates, assembling proteins from peptides, and protein quantification from peptides. MS/MS spectra were searched against a Uniprot human database (September 2016) with both the forward and reverse sequences. Database search criteria are as follows: tryptic with two missed cleavages, a precursor mass tolerance of 10 ppm, fragment ion mass tolerance of 0.6 Da, static alkylation of cysteine (57.02146 Da), static TMT labeling of lysine residues and N-termini of peptides (229.16293 Da), variable phosphorylation of serine, threonine and tyrosine (79.966 Da), and variable oxidation of methionine (15.99491 Da). TMT reporter ion intensities were measured using a 0.003 Da window around the theoretical *m/z* for each reporter ion in the MS^3 scan. Peptide spectral matches with poor quality MS^3 spectra were excluded from quantitation (summed signal-to-noise across 10 channels < 200 and precursor isolation specificity < 0.5). Only proteins containing at least two unique peptides identified in the experiment were included in final quantitation.

Chemistry Synthetic Scheme

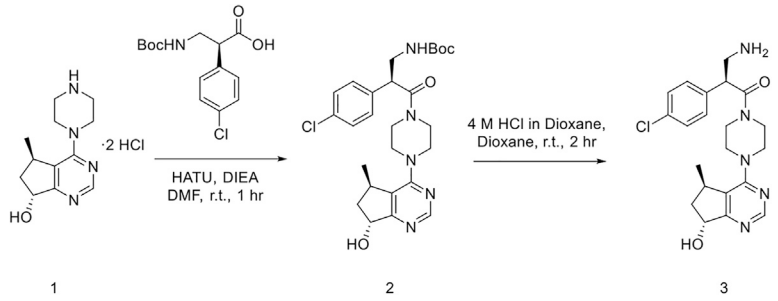

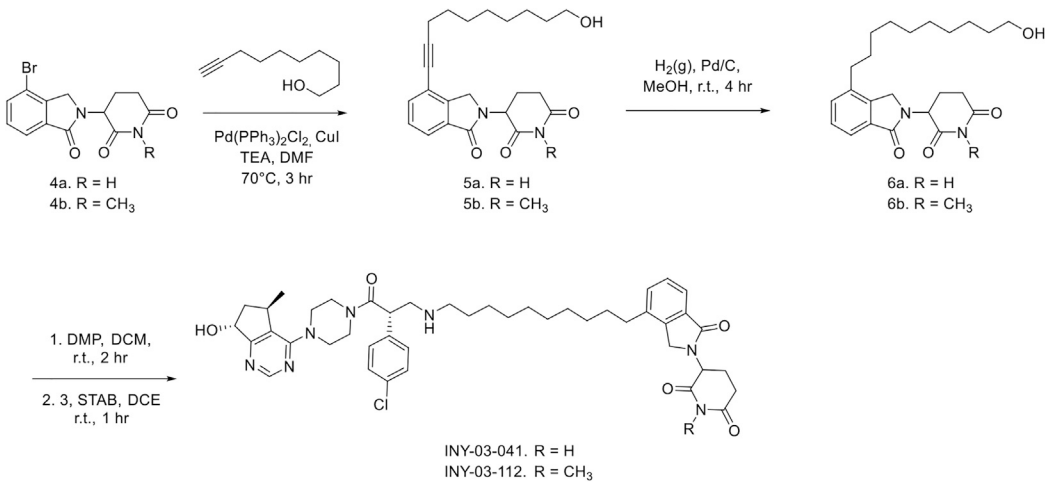

General Chemistry Methods

Reagents and solvents were purchased from commercial suppliers and were used without further purification unless otherwise noted. Reactions were monitored using a Waters Acquity UPLC/MS system (Waters PDA eλ Detector, QDa Detector, Sample manager - FL, Binary Solvent Manager) using Acquity UPLC® BEH C18 column (2.1 x 50 mm, 1.7 μm particle size): solvent gradient = 85% A at 0 min, 1% A at 1.7 min; solvent A = 0.1% formic acid in Water; solvent B = 0.1% formic acid in Acetonitrile; flow rate: 0.6 mL/min. Products were purified by flash column chromatography using CombiFlash®Rf with Teledyne Isco RediSep® normal-phase silica flash columns (4 g, 12 g, 24 g, 40 g or 80 g) and preparative HPLC using Waters SunFireTM Prep C18 column (19 x 100 mm, 5 μm particle size) using a gradient of 15-75% methanol in water containing 0.05% trifluoroacetic acid (TFA) over 48 min (60 min run time) at a flow of 40 mL/min. ^{1}H NMR spectra were recorded on 500 MHz Bruker Avance III spectrometer, and chemical shifts are reported in million (ppm, δ) downfield from tetramethylsilane (TMS). Coupling constants (J) are reported in Hz. Spin multiplicities are described as s (singlet), br (broad singlet), d (doublet), t (triplet), q (quartet) and m (multiplet). Purities of assayed compounds were in all cases greater than 95%, as determined by reverse-phase HPLC analysis.

Abbreviations Used

DCM: Dichloromethane
DIEA: N,N-Diisopropylethylamine
DMF: Dimethylformamide
TEA: Triethylamine
DMP: Dess–Martin periodinane
STAB: Sodium triacetoxyborohydride
DCE: 1,2-Dichloroethane
MeOH: Methanol

Chemical Synthesis of INY-03-041 and INY-03-112

Chemical Synthesis of 3

*Tert-butyl((S)-2-(4-chlorophenyl)-3-(4-((5R,7R)-7-hydroxy-5-methyl-6,7-dihydro-5H-cyclopenta[d]pyrimidin-4-yl)piperazin-1-yl)-3-oxopropyl)carbamate (**2**):*. To a solution of known intermediate **1** (Blake et al., 2012) (727 mg, 2.37 mmol), (S)-3-((tert-butoxycarbonyl)amino)-2-(4-chlorophenyl)propanoic acid (711 mg, 2.37 mmol) and HATU (902 mg, 2.37 mmol) in DMF (12 mL) was added DIEA (2.1 mL) and stirred for 1 hour at r.t. The reaction mixture was diluted ethyl acetate (30 mL) and washed with water (2 x 15 mL) and brine (2 x 15 mL). The organic layer was dried over anhydrous sodium sulfate, filtered, and concentrated in vacuo to afford **2** as a yellow oil (1.22 g, 100% yield). The crude was used directly for the next reaction. LC-MS: m/z 516.27 [M+1].

*(S)-3-amino-2-(4-chlorophenyl)-1-(4-((5R,7R)-7-hydroxy-5-methyl-6,7-dihydro-5H-cyclopenta[d]pyrimidin-4-yl)piperazin-1-yl)propan-1-one (**3**):*. To a solution of intermediate **2** (1.22 g, 2.37 mmol) in dioxane (7 mL) was added 4 M HCl in dioxane (5 mL). The reaction was stirred at r.t. for 4 hours. The reaction mixture was concentrated in vacuo and purified by reverse-phase HPLC (95-35% methanol in water) to obtain **3** as a TFA salt. The resultant TFA salt was dissolved in a mixture of 4:1 chloroform: isopropanol (50 mL) and washed with sat. aq sodium bicarbonate (50 mL) to give **3** as a white foam (868 mg, 88% yield). LC-MS: m/z 416.25 [M+1]. ^{1}H

NMR (500 MHz, DMSO-d6) δ 8.43 (s, 1H), 7.43 – 7.38 (m, 2H), 7.35 – 7.28 (m, 2H), 4.84 (t, J = 7.3, 6.2 Hz, 1H), 4.07 (dd, J = 8.3, 5.3 Hz, 1H), 3.73 – 3.66 (m, 1H), 3.64 – 3.56 (m, 3H), 3.52 – 3.35 (m, 4H), 3.22 – 3.16 (m, 1H), 3.09 (dd, J = 12.6, 8.3 Hz, 1H), 2.72 – 2.67 (m, 1H), 2.01 – 1.87 (m, 2H), 1.04 (dd, J = 6.5, 3.9 Hz, 3H).

Synthesis of INY-03-041 and INY-03-112

*3-(4-(10-hydroxydec-1-yn-1-yl)-1-oxoisoindolin-2-yl)piperidine-2,6-dione (**5a**).* Known intermediate **4a** (Zhou et al., 2018) (500 mg, 1.55 mmol), dec-9-yn-1-ol (478 mg, 3.10 mmol), $Pd(PPh_3)_2Cl_2$ (113 mg, 0.16 mmol) and CuI (61 mg, 0.32 mmol) were dissolved in TEA (4 mL) and DMF (8 mL). The reaction mixture was flushed with nitrogen (x3) and stirred at 70°C for 3 hours. The reaction mixture was cooled to r.t., diluted with ethyl acetate (50 mL) and filtered through celite. The organic layer was washed with brine (3 x 20 mL), dried over anhydrous sodium sulfate, filtered and concentrated in vacuo. The crude material was purified by column chromatography on silica gel (9:1 DCM:MeOH) to afford **5a** as a pale yellow solid (503 mg, 82% yield). LC-MS: m/z 397.24 [M+1]. ^{1}H NMR (500 MHz, DMSO-d6) δ 11.00 (s, 1H), 7.71 (dd, J = 7.6, 1.0 Hz, 1H), 7.64 (dd, J = 7.7, 1.0 Hz, 1H), 7.52 (t, J = 7.6 Hz, 1H), 5.76 (s, 2H), 5.15 (dd, J = 13.3, 5.2 Hz, 1H), 4.45 (d, J = 17.6 Hz, 1H), 4.31 (d, J = 17.6 Hz, 1H), 3.37 (t, J = 6.5 Hz, 2H), 2.92 (ddd, J = 17.3, 13.6, 5.5 Hz, 1H), 2.64 – 2.57 (m, 1H), 2.50 – 2.40 (m, 2H), 2.06 – 1.99 (m, 1H), 1.62 – 1.54 (m, 2H), 1.47 – 1.37 (m, 3H), 1.36 – 1.23 (m, 5H), 1.18 (t, J = 7.3 Hz, 1H).

*3-(4-(10-hydroxydecyl)-1-oxoisoindolin-2-yl)piperidine-2,6-dione (**6a**).* To a solution of intermediate **5a** (100 mg, 0.25 mmol) in MeOH (10 mL) was added Pd/C (10 mg). H_2 (g) was introduced to the reaction mixture, and the reaction was stirred at r.t. for 4 hours. The reaction mixture was filtered over celite and concentrated in vacuo to afford **6a** as a white solid (91 mg, 91% yield). LC-MS: m/z 401.30 [M+1]. ^{1}H NMR (500 MHz, DMSO-d6) δ 10.98 (s, 1H), 7.60 – 7.54 (m, 1H), 7.50 – 7.41 (m, 2H), 5.13 (dd, J = 13.3, 5.1 Hz, 1H), 4.45 (d, J = 17.2 Hz, 1H), 4.34 – 4.28 (m, 2H), 3.36 (td, J = 6.5, 4.9 Hz, 2H), 2.92 (ddd, J = 17.3, 13.7, 5.4 Hz, 1H), 2.66 – 2.58 (m, 3H), 2.43 (qd, J = 13.3, 4.5 Hz, 1H), 2.01 (dtd, J = 12.7, 5.2, 2.2 Hz, 1H), 1.66 – 1.54 (m, 2H), 1.43 – 1.35 (m, 2H), 1.33 – 1.21 (m, 12H).

*3-(4-(10-(((S)-2-(4-chlorophenyl)-3-(4-((5R,7R)-7-hydroxy-5-methyl-6,7-dihydro-5H-cyclopenta[d]pyrimidin-4-yl)piperazin-1-yl)-3-oxopropyl)amino)decyl)-1-oxoisoindolin-2-yl)piperidine-2,6-dione (**INY-03-41**).* To a solution of intermediate **6a** (83 mg, 0.21 mmol) in DCM (4 mL) was added DMP (132 mg, 0.31 mmol). The reaction was stirred at r.t. for 2 hours. The reaction mixture was filtered and concentrated in vacuo to obtain 10-(2-(2,6-dioxopiperidin-3-yl)-1-oxoisoindolin-4-yl)decanal (84 mg, quantitative yield). LC-MS: m/z 399.27 [M+1]. The crude material was then dissolved in DCE (2 mL), followed by addition of intermediate **3** (131 mg, 0.31 mmol). The reaction was stirred at r.t. for 30 minutes, after which STAB (89 mg, 0.42 mmol) was added. The reaction mixture was stirred for an additional 1 hour. The reaction was quenched by sat. aq sodium bicarbonate (10 mL) and extracted with DCM (3 x 20 mL). The organic layers were combined, dried over anhydrous sodium sulfate, filtered and concentrated in vacuo. The crude residue was purified by reverse-phase HPLC (75-15% methanol in water) to obtain **INY-03-041** (TFA salt). The resultant TFA salt was dissolved in 4:1 chloroform:isopropanol (10 mL) and washed with sat. aq sodium bicarbonate. The organic layer was dried over anhydrous sodium sulfate, filtered and concentrated in vacuo to afford title compound as an off-white solid (42 mg, 25% yield). LC-MS: m/z 798.42 [M+1]. ^{1}H NMR (500 MHz, DMSO-d6) δ 8.43 (s, 1H), 7.56 (dd, J = 5.4, 3.2 Hz, 1H), 7.45 – 7.43 (m, 2H), 7.41 (d, J = 8.2 Hz, 2H), 7.34 (d, J = 8.2 Hz, 2H), 5.38 (d, 1H), 5.13 (dd, J = 13.3, 5.1 Hz, 1H), 4.87 – 4.80 (m, 1H), 4.45 (d, J = 17.1 Hz, 1H), 4.29 (dd, J = 15.4, 7.6 Hz, 2H), 3.70 – 3.56 (m, 5H), 3.51 – 3.42 (m, 3H), 3.41 – 3.36 (m, 1H), 3.24 – 3.16 (m, 2H), 2.92 (ddd, J = 17.9, 13.8, 5.4 Hz, 1H), 2.77 – 2.71 (m, 1H), 2.63 (t, J = 7.5 Hz, 3H), 2.60 – 2.55 (m, 2H), 2.42 (tt, J = 13.3, 6.6 Hz, 1H), 2.04 – 1.93 (m, 2H), 1.93 – 1.87 (m, 1H), 1.62 – 1.55 (m, 2H), 1.41 – 1.35 (m, 2H), 1.32 – 1.26 (m, 4H), 1.22 (s, 8H), 1.03 (d, J = 6.8 Hz, 3H).

*3-(4-(10-hydroxydec-1-yn-1-yl)-1-oxoisoindolin-2-yl)-1-methylpiperidine-2,6-dione (**5b**).* **5b** was synthesized with similar procedures as **5a** using intermediate **4b** (90 mg, 0.27 mmol) as the starting material. **5b** was obtained as a light orange solid (49 mg, 44% yield). LC-MS: m/z 411.51 [M+1]. ^{1}H NMR (500 MHz, DMSO-d6) δ 7.71 (dd, J = 7.6, 1.0 Hz, 1H), 7.63 (dd, J = 6.8, 1.2 Hz, 1H), 7.52 (t, J = 7.6 Hz, 1H), 5.21 (dd, J = 13.5, 5.1 Hz, 1H), 4.44 (d, J = 17.6 Hz, 1H), 4.30 (d, J = 17.6 Hz, 1H), 3.36 (t, J = 6.5 Hz, 2H), 3.04 – 2.95 (m, 4H), 2.79 – 2.72 (m, 1H), 2.47 (t, J = 7.1 Hz, 2H), 2.45 – 2.39 (m, 1H), 2.03 (dtd, J = 12.7, 5.2, 2.2 Hz, 1H), 1.61 – 1.52 (m, 2H), 1.47 – 1.34 (m, 4H), 1.34 – 1.24 (m, 6H).

*3-(4-(10-hydroxydecyl)-1-oxoisoindolin-2-yl)-1-methylpiperidine-2,6-dione (**6b**).* **6b** was synthesized with similar procedures as **6a** using intermediate **5b** (42 mg, 0.1 mmol) as the starting material. **6b** was obtained as an off-white solid (33 mg, 79% yield). LC-MS: m/z 415.57 [M+1]. ^{1}H NMR (500 MHz, DMSO-d6) δ 7.60 – 7.53 (m, 1H), 7.49 – 7.43 (m, 2H), 5.20 (dd, J = 13.4, 5.1 Hz, 1H), 4.45 (d, J = 17.1 Hz, 1H), 4.32 – 4.27 (m, 2H), 3.36 (td, J = 6.6, 5.1 Hz, 2H), 3.01 (s, 3H), 3.00 – 2.95 (m, 1H), 2.79 – 2.74 (m, 1H), 2.66 – 2.61 (m, 2H), 2.48 – 2.39 (m, 1H), 2.08 – 1.98 (m, 1H), 1.63 – 1.56 (m, 2H), 1.43 – 1.34 (m, 2H), 1.32 – 1.22 (m, 12H).

*3-(4-(10-(((S)-2-(4-chlorophenyl)-3-(4-((5R,7R)-7-hydroxy-5-methyl-6,7-dihydro-5H-cyclopenta[d]pyrimidin-4-yl)piperazin-1-yl)-3-oxopropyl)amino)decyl)-1-oxoisoindolin-2-yl)-1-methylpiperidine-2,6-dione (**INY-03-112**).* **INY-03-112** was synthesized with similar procedures as **INY-03-041** using intermediate **6b** (27 mg, 0.07 mmol) as the starting material. **INY-03-112** was obtained as an off-white solid (9 mg, 16% yield). LC-MS: m/z 812.47 [M+1]. ^{1}H NMR (500 MHz, DMSO-d6) δ 8.43 (s, 1H), 7.57 (dd, J = 5.8, 2.8 Hz, 1H), 7.49 – 7.43 (m, 4H), 7.37 – 7.32 (m, 2H), 5.40 (d, J = 5.5 Hz, 1H), 5.21 (dd, J = 13.4, 5.1 Hz, 1H), 4.83 (q, J = 6.3 Hz, 1H), 4.45 (d, J = 17.1 Hz, 1H), 4.38 (dd, J = 8.9, 5.1 Hz, 1H), 4.29 (d, J = 17.1 Hz, 1H), 3.76 – 3.41 (m, 8H), 3.41 – 3.34 (m, 3H), 3.10 (t, J = 10.0 Hz, 1H), 3.01 (s, 3H), 2.99 – 2.95 (m, 1H), 2.83 – 2.73 (m, 3H), 2.63 (t, J = 7.7 Hz, 2H), 2.43 (qd, J = 13.2, 4.5 Hz, 1H), 2.05 – 1.87 (m, 3H), 1.59 (t, J = 7.5 Hz, 2H), 1.50 (s, 2H), 1.33 – 1.27 (m, 4H), 1.23 (s, 8H), 1.02 (d, J = 6.9 Hz, 3H).

QUANTIFICATION AND STATISTICAL ANALYSIS

Anti-proliferation Assay

Growth rate inhibition values were determined as described previously (Hafner et al., 2017) using python 3.7.3. Data was visualized using a non-linear regression curve fit in GraphPad Prism 8. N=3 biological replicates were used for each treatment condition and each data point represents the mean +/- SEM, as also indicated by the figure legend.

LC-MS Data Analysis

Reporter ion intensities were normalized and scaled using in house scripts and the R framework (Team, 2013). Statistical analysis was carried out using a moderated t-test in the limma package within the R framework (Ritchie et al., 2015).

DATA AND CODE AVAILABILITY

The accession number for the proteomic data reported in this paper is Pride: PXD015207.